X-mode beam broadening in turbulent plasma

P. Tretinnikov[1,2], E. Gusakov[1], S. Heuraux[2]
1 Ioffe Institute, 194021 Saint-Petersburg, Russia
2 Institut Jean Lamour, U. de Lorraine-CNRS 54011 Nancy, France

It is shown that plasma turbulence at the edge of a fusion machine can lead to significant broadening of an X-mode microwave beam, which impacts the performance of the heating systems and diagnostics as well. Based on the similar method developed for the O-mode polarization, the expression for mean microwave power distribution after the beam passing through the plasma edge turbulence is obtained, its spatial and probabilistic distributions are analysed. As this polarization is used for the coherent Thomson Scattering (CTS) on ITER and for the electron cyclotron resonance heating (ECRH) on ASDEX Upgrade, numerical simulations of beam broadening due to the edge turbulence are performed for the two conditions of plasma parameters, related to the planned CTS experiments on ITER and to ECRH experiments on ASDEX Upgrade. Ideas to reduce the beam broadening induced by the edge turbulence in the CTS case have been tested and summarized in the conclusions.

Introduction.

High-frequency electromagnetic beams are widely used in thermonuclear fusion research as a tool of localised plasma heating and current drive, for instance the methods of electron cyclotron resonance heating (ECRH) [1] and electron cyclotron current drive (ECCD) [2]. Another domain of applications using quasi-optical electromagnetic beams in nuclear fusion is plasma diagnostics, possessing high spacial resolution, such as collective Thomson scattering (CTS) [3] and Doppler reflectometry [4]. Propagation of slightly divergent beams is relatively easy to analyse, its field distribution can be precisely predicted for given smooth plasma density and magnetic field profiles. Nevertheless, it was demonstrated that presence of plasma edge turbulence is able to significantly disturb a beam launched from outside [5-9].

Neoclassical tearing modes (NTMs) increase locally the radial transport that degrades the plasma performance, that is why NTMs suppression is required for a fusion reactor operation. Precise position and intensity of the current drive influence the efficiency of the NTMs suppression [8,10-12]. The energy deposition profile broadening, associated with a launched beam broadening, can lead to the reduction of the stabilization efficiency. In terms of the microwave plasma diagnostics the probing beam broadening results in deterioration of the spatial resolution and it may complicate the diagnostic data interpretation. Experimental conformation of the broadened ECRH deposition was observed for DIII-D tokamak [13]. The microwave power scattering off blobs and the edge turbulence was also experimentally examined on TORPEX [14, 15] and TCV tokamak [16, 17]

correspondingly. To take into account the role of the plasma turbulence in the beam propagation several methods were developed. Statistical description of EC wave scattering, based on the Fokker-Planck equation, was derived in [18]. This model describes a ray trajectory diffusion on blobs as a multi-scattering process. This approach implies specific structure of the blobs and allows to obtain rather a relevant estimation for an average beam broadening. Several numerical codes were developed with respect to the effect of a beam scattering off the turbulence: WKBeam [19], IPF-FDMC [20], EMIT-3D [21], COMSOL [22], FWR2D and FWR3D [6]. Propagation of an ordinary polarized (O-mode) beam in turbulent plasma was analysed analytically and numerically in [5]. It was demonstrated that the presence of a turbulent edge layer can result in a drastic distortion of the beam shape depending on turbulence amplitude. The developed analytical approach allowed to describe averaged geometrical beam characteristics in turbulent plasma. Corresponding recommendation for ITER ECRH experiments were done especially in the case of NTM control where the beam width is crucial to reach the magnetic island with power deposition at the right position.

In this work we apply the developed method, based on eikonal perturbation analysis, for describing propagation and scattering process of an extraordinary polarized (X-mode) beam in turbulent plasmas. In particular the results are discussed in terms of possible problems for the CTS experiments on ITER. Statistical properties of the beam are considered in regimes with strong turbulence, probabilistic distribution function of the intensity is obtained that allows to provide statistical analysis of processes associated with the wave-plasma energy exchange in turbulent plasmas. The paper is organized as follows: in the first section we present analytical approach of describing an X-mode beam propagating in magnetized turbulent plasma. Numerical analysis, harnessing full-wave code, and comparison with the theory are illustrated in the second section. The main results are discussed in the last section.

1 X-mode beam broadening in turbulent plasma. Analytical description.

In this section we consider a microwave X-mode beam 2D propagation in turbulent inhomogeneous magnetised plasma analytically. Plasma edge of a fusion machine is regarded in the model of Cartesian coordinates. Direction of plasma inhomogeneity is along x axis and coincides with direction of the beam propagation, z axis corresponds to lines of external magnetic field $\mathbf{B}$. Considering electromagnetic waves possessing the extraordinary polarization and propagating perpendicularly to the external magnetic field in absence of the upper hybrid resonance the wave equation

$$\frac{\partial^2}{\partial x_j \partial x_j} E_i - \frac{\partial^2}{\partial x_i \partial x_j} E_j + \frac{\omega^2}{c^2} \varepsilon_{ij} E_j = 0 \tag{1}$$

can be written as

$$\left[\frac{\partial^2}{\partial x^2} + \frac{\partial^2}{\partial y^2} + k^2(x) + \delta k^2(x,y) \right] E_y = 0 \tag{2}$$

where ε_{ij} is plasma dielectric tensor, the X-mode wave number $k^2 = \frac{\omega^2}{c^2} \frac{\varepsilon^2 - g^2}{\varepsilon}$,
$\varepsilon = 1 - \frac{\omega_{pe}^2}{\omega^2 - \omega_{ce}^2}$ and $g = \frac{\omega_{ce}}{\omega} \frac{\omega_{pe}^2}{\omega^2 - \omega_{ce}^2}$ are components of the dielectric tensor in the cold-

plasma approximation, ω - probing frequency, ω_{pe} - plasma frequency, ω_{ce} - electron cyclotron frequency, $\delta k^2 = -\frac{\omega_{pe}^2}{c^2}\frac{\left(\omega^2-\omega_{ce}^2\right)\left(\omega^2-2\omega_{pe}^2\right)+\omega_{pe}^4}{\left(\omega^2-\omega_{ce}^2-\omega_{pe}^2\right)^2}\frac{\delta n}{n}$, n - background plasma density and δn - 2D fluctuation of the density. The equation (2) can be analysed by means of the geometrical optics approach, to this we consider the electric field in the form

$$E_y = E_{y0}e^{i\psi(x,y)} \tag{3}$$

$\psi(x,y)$ is the eikonal. This form corresponds to a plane wave locally $\psi(x_0+x, y_0+y) \approx x\frac{\partial\psi}{\partial x}(x_0,y_0) + y\frac{\partial\psi}{\partial y}(x_0,y_0)$. The eikonal equation reads as

$$K_x^2 + K_y^2 = k^2(x) + \delta k^2(x,y) \tag{4}$$

where the introduced wave numbers $K_{x_j} = \frac{\partial\psi}{\partial x_j}$, $j = \{1,2\}$ numerates the two directions. Assuming that the fluctuations level is small $\delta k^2 \ll k^2$ we can use the perturbation method and consider the wave numbers as $K_{x_j} = k_{x_j} + \delta k_{x_j}$, where k_{x_j} is the wave number for plasma without the turbulence, δk_{x_j} is the correction associated with the turbulence. These values are specified as follows

$$k_x^2 + k_y^2 = k^2(x) \tag{5}$$

$$\delta k_x + \delta k_y \frac{k_y}{k_x} = \frac{1}{2k_x(x)}\delta k^2(x,y) \tag{6}$$

The ray trajectory ($y = y(x)$) is determined by the unperturbed part $\frac{dy}{dx} = \frac{k_y}{k_x}$. Taking into account that $k(x)$ is a function of the radial coordinate only k_y is a constant on the ray trajectory. Then we can write down the eikonal explicitly

$$\psi(x,y;k_y) = \int^x dx'\left[k_x(x') + \delta k_x(x', y'(x'))\right] + yk_y + \int^x dx'\frac{dy'}{dx'}\delta k_y(x', y'(x')) \tag{7}$$

using the equations (5,6)

$$\psi(x,y;k_y) = \int^x dx'\sqrt{k^2(x') - k_y^2} + yk_y + \frac{1}{2}\int^x dx'\frac{\delta k^2(x', y'(x'))}{k_x}(x') \tag{8}$$

A probing electromagnetic beam represents a sum of poloidal harmonics numerated by the poloidal wave numbers k_y at the plasma edge. Each harmonic possesses amplitude

$$E_{y0}(k_y) = \int_{-\infty}^{+\infty} dy E_y(x=0,y)\, e^{-ik_y y} \tag{9}$$

(at the plasma edge) and can be described by the presented method of the geometrical optics. Considering an initially gaussian beam $E_y(x=0,y) = Ee^{-\frac{y^2}{\delta^2}}$ the explicit expression for the amplitude

$$E_{y0}(k_y) = E\sqrt{\pi}\delta e^{-\frac{k_y^2\delta^2}{4}} \tag{10}$$

Then the electric field distribution for the whole beam

$$E_y(x,y) = \int_{-\infty}^{+\infty}\frac{dk_y}{2\pi}E_{y0}(k_y)\sqrt{\frac{c}{\omega k_x(x)}}e^{i\psi(x,y;k_y)} \tag{11}$$

here the coefficient $\sqrt{\frac{c}{\omega k_x(x)}}$ describes the energy flux conservation. Substituting the eikonal (8) into (11) and using the paraxial approximation $k_x \approx k\left(x\right) - \frac{k_y^2}{2k(x)}$ we obtain

$$E_y\left(x,y\right) = \int_{-\infty}^{+\infty} \frac{dk_y}{2\pi} E_{y0}\left(k_y\right) \sqrt{\frac{c}{\omega k\left(x\right)}} e^{ik_y y} e^{i\int_0^x dx' k(x') - i\frac{k_y^2 d(x)^2}{2} + i\delta\phi} \tag{12}$$

the used notation $d(x)^2 = \int_0^x dx' \frac{1}{k(x')}$, the random phase $\delta\phi = -\int_0^x dx' \kappa(x') \frac{\delta n(x', y'(x,y,x',k_y))}{n(x')}$, $\kappa(x) = \frac{1}{k(x)} \frac{\omega_{pe}^2}{2c^2} \frac{\left(\omega^2 - \omega_{ce}^2\right)\left(\omega^2 - 2\omega_{pe}^2\right) + \omega_{pe}^4}{\left(\omega^2 - \omega_{ce}^2 - \omega_{pe}^2\right)^2}$. This phase perturbation of a partial wave adds up along the wave trajectory according to the geometrical optics $y'(x,y,x',k_y) = y - k_y l^2(x',x)$, $l^2(x',x) = \int_{x'}^x ds \frac{1}{k(s)}$.

In accordance with (12) the beam passing through turbulent plasma is the more distorted the higher turbulence level. Nevertheless, taking into account random behaviour of the phase perturbation, it is possible to define average and probabilistic characteristics of the beam. To this we consider averaged intensity of a beam

$$\left\langle E_y^2\left(x,y\right)\right\rangle = \int_{-\infty}^{+\infty} \frac{dk_{y_1} dk_{y_2}}{\left(2\pi\right)^2} E_{y0}\left(k_{y_1}\right) E_{y0}^*\left(k_{y_2}\right) \frac{c}{\omega k\left(x\right)} \times$$
$$e^{i\left(k_{y_1} - k_{y_2}\right)y} e^{-\frac{i\left(k_{y_1}^2 - k_{y_2}^2\right)d(x)^2}{2}} \left\langle e^{i\left(\delta\phi\left(x,y,k_{y_1}\right) - \delta\phi\left(x,y,k_{y_2}\right)\right)}\right\rangle \tag{13}$$

The random phase $\delta\phi$ represents sum of random values acquired on a scale of turbulence correlation length that implies the turbulence layer to be larger than several correlation lengths. Thus $\delta\phi$ obeys the normal distribution, that results in

$$\left\langle E_y^2\left(x,y\right)\right\rangle = \int_{-\infty}^{+\infty} \frac{dk_{y_1} dk_{y_2}}{\left(2\pi\right)^2} E_{y0}\left(k_{y_1}\right) E_{y0}^*\left(k_{y_2}\right) \frac{c}{\omega k\left(x\right)} \times$$
$$e^{i\left(k_{y_1} - k_{y_2}\right)y} e^{-\frac{i\left(k_{y_1}^2 - k_{y_2}^2\right)d(x)^2}{2}} e^{-\frac{\left\langle\left(\delta\phi(x,y,k_{y_1}) - \delta\phi(x,y,k_{y_2})\right)^2\right\rangle}{2}} \tag{14}$$

To evaluate

$$\left\langle \delta\phi\left(x,y,k_{y_i}\right) \delta\phi\left(x,y,k_{y_j}\right)\right\rangle = \int_0^x \int_0^x dx' dx'' \kappa(x') \kappa(x'') \times$$
$$\left\langle \frac{\delta n(x', y'(x,y,x',k_{y_i}))}{n(x')} \frac{\delta n(x'', y'(x,y,x'',k_{y_j}))}{n(x'')} \right\rangle \tag{15}$$

we introduce relative radial coordinates $X = \frac{x'+x''}{2}$, $\Delta = x' - x''$, local relative turbulence amplitude $\frac{\delta\tilde{n}(x)}{n(x)}$ and cross-correlation function $CCF(x,y)$ according to the definition

$$\left\langle \frac{\delta n(x', y'(x,y,x',k_{y_i}))}{n(x')} \frac{\delta n(x'', y'(x,y,x'',k_{y_j}))}{n(x'')} \right\rangle =$$
$$\frac{\delta\tilde{n}^2(X)}{n^2(X)} CCF(\Delta, y'(x,y,X,k_{y_i}) - y'(x,y,X,k_{y_j})) \tag{16}$$

Introducing this definition we supposed that the cross-correlation function is the function of the coordinates difference only and homogeneous in space. Then

$$\left\langle \delta\phi\left(x,y,k_{y_i}\right)\delta\phi\left(x,y,k_{y_j}\right)\right\rangle = \int_0^x dX\kappa^2(X)\frac{\delta\tilde{n}^2(X)}{n^2(X)}\times \int \frac{dq_y}{2\pi}\left|n_{0,q_y}\right|^2 e^{iq_y(y'(x,y,X,k_{y_i})-y'(x,y,X,k_{y_j}))} \tag{17}$$

where $\left|n_{q_x,q_y}\right|^2 = \int \frac{d\Delta x d\Delta y}{4\pi^2} CCF\left(\Delta x,\Delta y\right)e^{-i\Delta x q_x - i\Delta y q_y}$ is Fourier spectrum of the turbulence. Using the explicit form for $y'(x,y,x',k_y)$, the exponential factor in the equation (14)

$$\left\langle \left(\delta\phi\left(x,y,k_{y_1}\right)-\delta\phi\left(x,y,k_{y_2}\right)\right)^2\right\rangle = 2\int_0^x dX\kappa^2(X)\frac{\delta\tilde{n}^2(X)}{n^2(X)}\times \int \frac{dq_y}{2\pi}\left|n_{0,q_y}\right|^2\left[1-e^{iq_y l^2(X,x)(k_{y_2}-k_{y_1})}\right] \tag{18}$$

moreover assuming a symmetric spectrum of the turbulence $\left|n_{0,q_y}\right|^2 = \left|n_{0,-q_y}\right|^2$ we obtain the expression

$$\left\langle \left(\delta\phi\left(x,y,k_{y_1}\right)-\delta\phi\left(x,y,k_{y_2}\right)\right)^2\right\rangle = 2\int_0^x dX\kappa^2(X)\frac{\delta\tilde{n}^2(X)}{n^2(X)}\times \int \frac{dq_y}{2\pi}\left|n_{0,q_y}\right|^2\left[1-\cos\left(q_y l^2\left(X,x\right)\left(k_{y_2}-k_{y_1}\right)\right)\right] \tag{19}$$

It is seen that in the strong turbulence regime $\left\langle\delta\phi^2\left(x,y,k_y\right)\right\rangle \gg 1$ only small argument values of the cosine in (19) contributes to the integral expression (14), then, keeping the two first terms of the cosine expansion in (19), the averaged difference of the phase perturbations becomes

$$\left\langle \left(\delta\phi\left(x,y,k_{y_1}\right)-\delta\phi\left(x,y,k_{y_2}\right)\right)^2\right\rangle = \int_0^x dX\kappa^2(X)l^4\left(X,x\right)\frac{\delta\tilde{n}^2(X)}{n^2\left(X\right)}\times \int \frac{dq_y}{2\pi}\left|n_{0,q_y}\right|^2 q_y^2\left(k_{y_1}-k_{y_2}\right)^2 \tag{20}$$

Substituting (20) into (14) and calculating standard integrals we finally obtain

$$\left\langle E_y^2\left(x,y\right)\right\rangle = E^2\frac{\omega}{ck\left(x\right)}\frac{\delta}{\sqrt{2}W\left(x\right)}e^{-\frac{y^2}{W^2(x)}} \tag{21}$$

the averaged beam width

$$W^2\left(x\right) = \frac{\delta^2}{2}+\frac{2d^4\left(x\right)}{\delta^2}+4\int^x D(x')l^4(x,x')dx' \tag{22}$$

where $D(x) = \frac{1}{2}\kappa^2(X)\frac{\delta\tilde{n}^2(X)}{n^2(X)}\int\frac{dq_y}{2\pi}\left|n_{0,q_y}\right|^2 q_y^2$. The first term in equation (22) stands for the initial beam width, the second one represents diffraction taking into account refractive index in inhomogeneous medium, the third term describes the effect of beam broadening in turbulent plasma. To analyse impact of the turbulence on the beam broadening we

estimate the third term in (22) $W^2_{Xturb} = 4\int^x D(x')l^4(x,x')dx'$ at position beyond the periphery turbulence layer $x > x_{turb}$, where x_{turb} is the width of this layer,

$$W^2_{Xturb} \approx \frac{1}{2} d^4(x) x_{turb} \int \frac{dq_y}{2\pi} \left|n_{0,q_y}\right|^2 q_y^2 \times$$
$$\left\langle \frac{\omega_{pe}^4}{c^2} \frac{\left(\left(\omega^2-\omega_{ce}^2\right)\left(\omega^2-2\omega_{pe}^2\right)+\omega_{pe}^4\right)^2}{\left(\omega^2\left(\omega^2-\omega_{ce}^2-\omega_{pe}^2\right)+\omega_{pe}^2\left(\omega_{pe}^2-\omega^2\right)\right)\left(\omega^2-\omega_{ce}^2-\omega_{pe}^2\right)^3} \frac{\delta\tilde{n}^2}{n^2} \right\rangle_{x_{turb}} \tag{23}$$

$\langle ... \rangle_{x_{turb}}$ denotes averaging over the turbulence layer. Comparing the second term in (22) with (23) one can see that the turbulence at plasma edge results in an effectively larger diffraction for an averaged beam. Assuming that the cross-correlation function $CCF(\Delta x, \Delta y)$ is monotonous, we can deduce that $\int \frac{dq_y}{2\pi} \left|n_{0,q_y}\right|^2 q_y^2 \sim \frac{\lambda_{cx}}{\lambda_{cy}^2}$, where λ_{cx} and λ_{cy} are radial and poloidal correlation lengths correspondingly determined as $CCF(\lambda_{cx}, 0) = CCF(0, \lambda_{cy}) = e^{-1}$. Thus we know how parameters of the turbulence influence the beam broadening

$$W^2_{Xturb} \propto \delta\tilde{n}^2_{max} x_{turb} \frac{\lambda_{cx}}{\lambda_{cy}^2} \tag{24}$$

$\delta\tilde{n}_{max}$ is the maximum of the turbulence amplitude for the sake of concreteness. Dependence of W^2_{Xturb} on plasma parameters and probing frequency is more complicated and described by the relative relations of $\omega, \omega_{ce}, \omega_{pe}$ in (23), also it should be noticed that the W^2_{Xturb} is independent on the initial beam width. The eq. (23) implies that the edge turbulence contribute to the beam broadening the most. Nevertheless the eq. (22) takes into account even the turbulence in the plasma core. Taking into account that typically the edge turbulence amplitude is much higher than in the plasma core and the correlation length is smaller at the peripheral plasma we can consider the edge turbulence as the main factor of the beam broadening. But one should keep in mind that it is not always the case [23].

The equations (21) and (22) specify the spatial distribution of an averaged X-mode beam in turbulent magnetized plasma. To obtain the probabilistic distribution of the intensity, considering the integral over poloidal wave numbers in (12) as a sum of random values, we assume that the electric field is normally distributed

$$f_E\left[E\left(x,y\right)\right] = \frac{1}{\sqrt{2\pi\left\langle E^2\left(x,y\right)\right\rangle}} e^{-\frac{\left(E(x,y)-\left\langle E(x,y)\right\rangle\right)^2}{2\left\langle E(x,y)^2\right\rangle}} \tag{25}$$

the dispersion of this distribution is the derived expression (21). Moreover the average electric field sharply decreases in the strong turbulence regime $\langle\delta\phi^2\rangle \gg 1$

$$\frac{\left\langle E\left(x,y\right)\right\rangle}{E\left(x,y\right)\Big|_{\delta n=0}} = e^{-\frac{\left\langle\delta\phi^2\right\rangle}{2}} \tag{26}$$

hence $\langle E\left(x,y\right)\rangle$ is negligible. The expression (25) represents parametric distribution of the electric field for each space position (x,y). The distribution function of intensity

$f_{E^2}\left[E^2\left(x,y\right)\right]$ is defined by equalizing the probabilities $dE^2 f_{E^2}\left[E^2\left(x,y\right)\right] = dE f_E\left[E\left(x,y\right)\right] + dE f_E\left[-E\left(x,y\right)\right]$, then

$$f_{E^2}\left[E^2\left(x,y\right)\right] = \frac{1}{\sqrt{2\pi\left\langle E^2\left(x,y\right)\right\rangle}} \frac{1}{\sqrt{E^2\left(x,y\right)}} e^{-\frac{E^2(x,y)}{2\left\langle E(x,y)^2\right\rangle}} \tag{27}$$

It should be mentioned that the probability of the relative deviation of intensity over its average value $I = \frac{E(x,y)^2}{\left\langle E(x,y)^2\right\rangle}$ is homogeneous in space and independent on plasma and turbulence parameters since the strong turbulence condition holds:

$$f_I\left[I\right] = \frac{1}{\sqrt{2\pi I}} e^{-\frac{I}{2}} \tag{28}$$

The distribution function for a microwave X-mode beam describes probability of the beam energy allocation in plasma volume, that allows to provide statistical analysis of processes associated with the wave-plasma energy exchange in strongly turbulent plasmas. A parametric decay instability is a typical example of such processes, and it will be analysed in works to follow.

2 Numerical results.

Numerical simulations of a high-frequency X-mode beam propagation in turbulent plasma provide comparison with the theoretical results established in the previous section. For the both types of the numerical simulations in this section (typical conditions for a CTS experiment on ITER and an ECRH experiment on Asdex Upgrade) the following applicability criteria of the analytical expressions, derived in the previous section, are fulfilled: the slab model is good for considering a beam propagation through a narrow turbulent layer, especially for reactor-size machines; the geometrical optics approach $\frac{d\lambda}{dx} \ll 2\pi$ holds since there is no cut off and resonance for a probing wave under the considered conditions, the turbulence typical scale (correlation length) is bigger than the probing wave length; low turbulence rate $\delta k^2 \ll k^2$ holds almost always for a realistic turbulence amplitude in a fusion machine, other than the the case when the turbulence is located in the vicinity of the upper-hybrid (UH) resonance since $\frac{\delta k^2}{k^2} \propto \frac{1}{\omega^2 - \omega_{ce}^2 - \omega_{pe}^2}$. In the simulated plasmas the UH resonance for the probing frequencies does not take place. The main parameter which influence the analytical applicability is the phase variation $< \delta\phi^2 >$. The numerical experiments described further in this section are performed in order to verify over which turbulence parameters domain the obtained analytical expressions are applicable ($< \delta\phi^2 > \gg 1$) in the framework of typical conditions for the CTS and the ECRH experiments, to evaluate the deviation from these expressions, to estimate significance of a beam broadening, caused by the plasma turbulence.

The simulations are performed using the full-wave code IPF-FD3D, this code corresponds to a Maxwell equations solver coupled to a J-solver which provide the linear response of magnetized plasma excited by a propagating wave. [24].

Simulations under the conditions of CTS experiment for ITER

For the first stage of simulations plasma parameters are chosen to be close to the expected ones for the ITER Baseline Scenario. By this choice we aim at modeling relevant condi-

tions for the planned CTS experiments on ITER. Value of magnetic field at the plasma center $B = 5.3$ T, central density $n_{max} = 1.3 \cdot 10^{20}$ m^{-3}. The model profiles are illustrated in figure 1. The probing frequency $f = 64$ GHz. These characteristics being representative

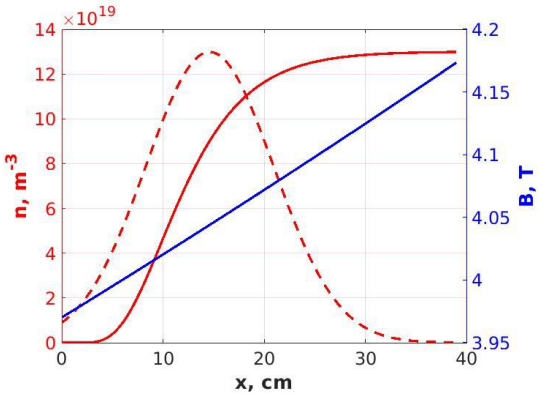


Рис. 1: Solid red and blue curves are density and magnetic field profiles respectively, dashed curve is envelope of the turbulence $\sqrt{\langle \delta n^2(x) \rangle}$ normalized to the maximal value of the background density

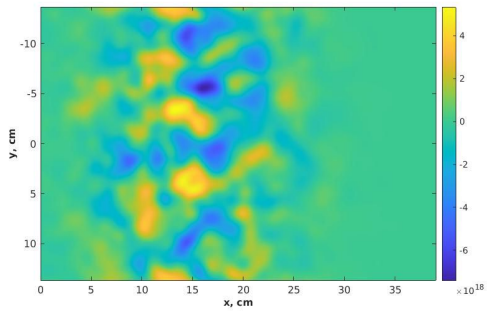


Рис. 2: One example of the turbulence map in the computation domain, the turbulence amplitude $\frac{\delta \tilde{n}_{max}}{n_{max}} = 1.7\%$ and the correlation length λ_c=1.6 cm

of ITER CTS [25], it becomes relevant to describe the impact of the edge turbulence on the measurements in the framework of the presented inputs. In particular the turbulence properties are extrapolated from existing experiments assuming that they are relevant for this work due to the fact the ITER edge turbulence properties are still unknown. This is the reason why the simulations of beam propagation were performed for different values of relative turbulence amplitude defined as $\frac{\delta \tilde{n}_{max}}{n_{max}} = \frac{\sqrt{\langle \delta n^2 \rangle_{max}}}{n_{max}}$ and correlation length λ_c which was assumed equal for radial and poloidal directions for simplicity $\lambda_c = \lambda_{cx} = \lambda_{cy}$, but could be performed without this assumption. The used range of the turbulence parameters for these simulations is $\frac{\delta \tilde{n}_{max}}{n_{max}} \in [0.9, 5.0]$ % and $\lambda_c \in [0.8, 6.4]$ cm. The choice of these parameters is aimed at: (I) checking the analytical expression in the wide range of the turbulence parameters, (II) covering the typical range of the turbulence parameters for a fusion machine so far as it is hard to predict what the turbulence properties will be in ITER.

The turbulence was generated on the base of 2D inverse fast Fourier transformation (IFFT2D), $\delta n(x, y) = \sqrt{\langle \delta n^2(x) \rangle} IFFT2D\left(S_{2D}(q_x, q_y) e^{i\xi}\right)$, $S_{2D}(q_x, q_y)$ is 2D matrix of the turbulence spectrum, ξ is the same size matrix of random phases, $\sqrt{\langle \delta n^2(x) \rangle}$ is the used turbulence envelope illustrated on figure 1 (normalized to n_{max}), amplitude of the envelope corresponds to the definition of the turbulence amplitude mentioned above. The usual model of symmetric turbulence spectrum was used $S_{2D}(q_x, q_y) = S_{2D}(q_\perp)$. The spectrum is constructed taking into account experimental data obtained on ASDEX Upgrade [26]. We applied the turbulence spectrum possessing the same shape (figure 3) but with a shifted knee position $q_\perp \rho_i = 1$, following the standard description of the turbulence k-spectrum [27], ρ_i is the ion Larmor radius, in accordance with higher ion temperatures in ITER plasmas, $T_i \approx 12$ keV. So far as the saturation level q_{sat} is unspecified in the experimental spectrum measurements, this offers us the possibility to adapt the spectrum through the q_{sat} parameter to access to the wanted correlation length. An example of the turbulence distribution is shown on figure 2 for the following parameters:

the turbulence amplitude $\frac{\delta\tilde{n}_{max}}{n_{max}} = 1.7\%$ and the correlation length λ_c=1.6 cm which is symmetric ($\lambda_c = \lambda_{cx} = \lambda_{cy}$) in accordance with the symmetric turbulence spectrum. The cross-correlation function is monotonous in the described turbulence model so the definition of the correlation length is chosen as $CCF\,(0, \lambda_c) = CCF\,(\lambda_c, 0) = e^{-1}$.

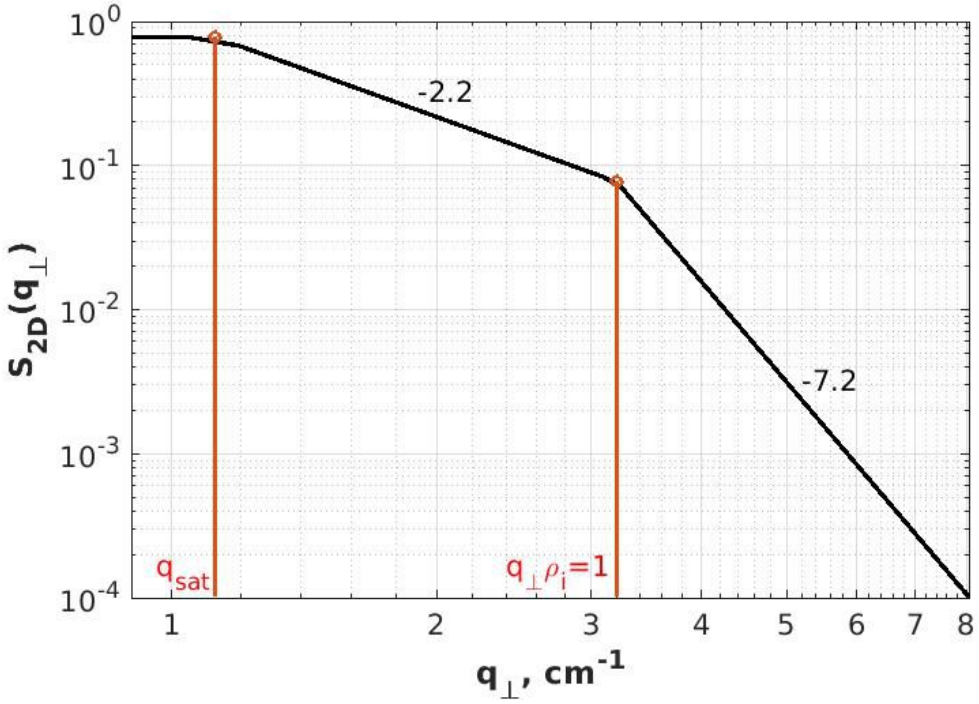


Рис. 3: Generic model of generated turbulence spectra

The results of numerical calculations of the averaged beam width $W(x)$ (see Eq. (22)) under the condition of a fixed turbulence correlation length $\lambda_c = 1.6$ cm and different turbulence amplitudes are shown on figure 4. The four simulated cases were done for different conditions in terms of applicability of the analytical description $\langle\delta\phi^2\rangle \gg 1$. For the turbulence level 0.9% the analytical description does not work well, for 1.7% it is at the border of the applicability criteria, for 3.5% and 5.0% the strong turbulence criteria holds well figure 5. One can see that the consistency between the numerical and analytical curves is in a good agreement with the applicability criteria, namely the higher $\langle\delta\phi^2\rangle$ value, the smaller relative discrepancy between the analytical and numerical beam broadening associated with the turbulence. The averaged beam width was analogously compared for different correlation lengths at fixed turbulence level $\frac{\delta\tilde{n}_{max}}{n_{max}} = 3.5\%$ figure 6. Averaging was performed over 400 realizations for each case, which provides confident results with a statistical error bars of 5%.

It is seen that presence of the edge turbulence, even possessing a low amplitude, can lead to significant beam spreading and increasing its angular width. In terms of diagnostics that results in a complication of interpretation the microwave diagnostics data and requires the knowledge of the edge turbulence properties. It also deteriorates the spatial resolution of the wave-based diagnostics.

To mitigate these negative effects it is worth considering the use of higher frequencies for the wave-based diagnostics such as CTS for ITER. For instance the evolution of three identical beams with different frequencies in turbulent plasma is presented on figure 7, the

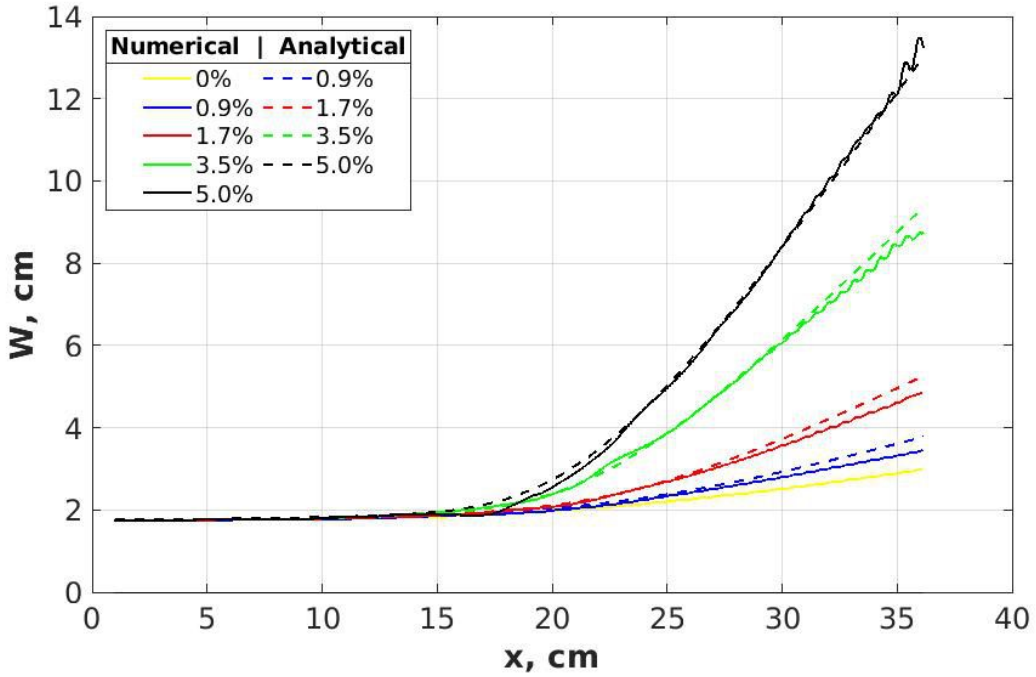


Рис. 4: Averaged beam width evolution in turbulent plasma for a fixed turbulence correlation length $\lambda_c = 1.6$ cm and different turbulence normalized amplitudes given in % $\frac{\delta\tilde{n}_{max}}{n_{max}}$

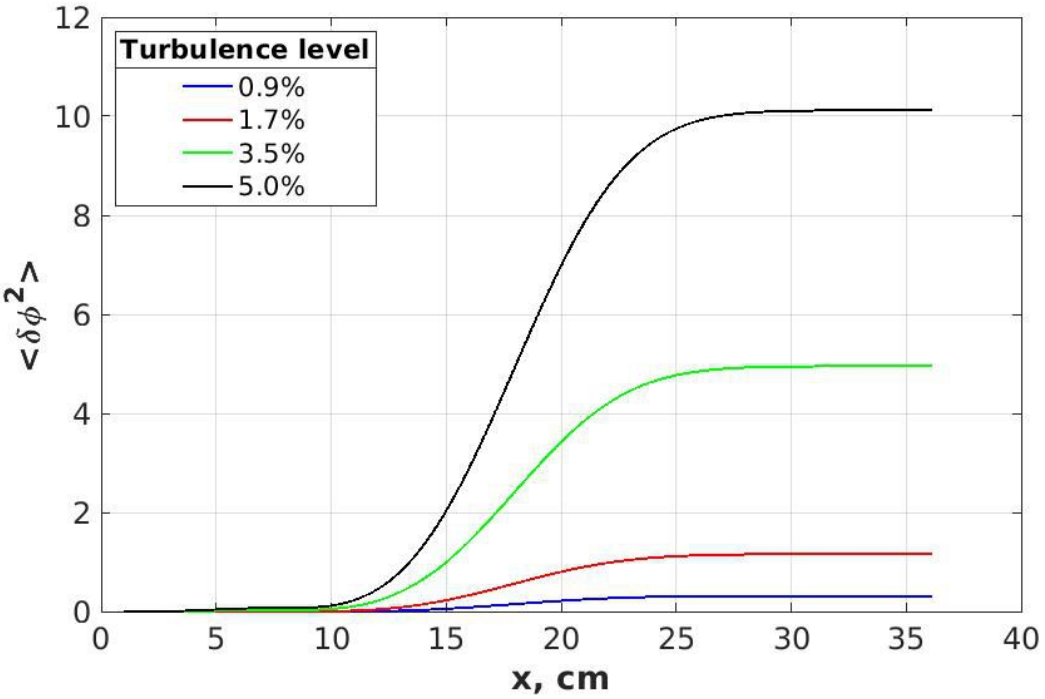


Рис. 5: Averaged square of the phase perturbations for different turbulence normalized amplitudes $\frac{\delta\tilde{n}_{max}}{n_{max}}$ measured in percentage

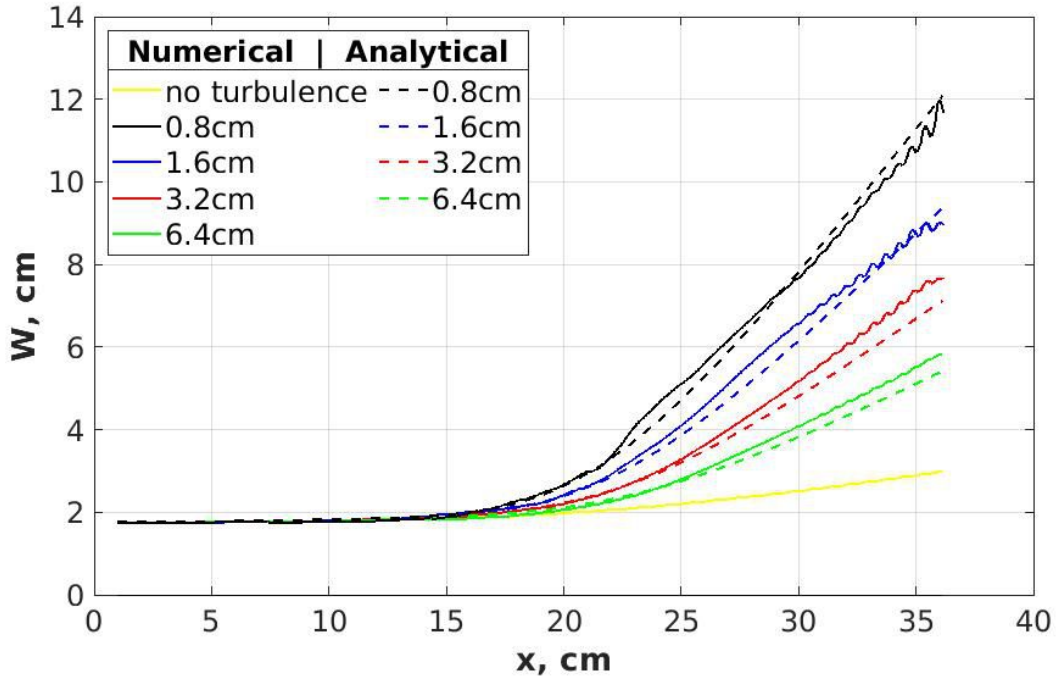


Рис. 6: Averaged beam width evolution in turbulent plasma for a fixed turbulence level $\frac{\delta\tilde{n}_{max}}{n_{max}} = 3.5\%$ and different correlation lengths λ_c values which specified for each analytical and numerical curve in cm

turbulence normalized amplitude 5.0%, the correlation length $\lambda_c = 1.6$ cm, the tested frequencies are $F = 64$ GHz, $F = 82$ GHz and $F = 100$ GHz. It is clearly seen that the higher probing frequency the less distortion of a probing beam under the considered conditions of typical parameters for the planned CTS experiment on ITER. The presented numerical results for the chosen three frequencies are aimed only at illustrating the beam broadening sensitivity to the probing frequency under the typical conditions for the planned CTS experiment on ITER. Here we do not propose using some optimal frequency because of the lack of the first-principle predictions about the characteristics of the ITER pedestal and the edge turbulence. This task requires rather precise (not typical) profiles and probably taking into account the real geometry for a concrete experiment.

The significant sensitivity to the frequency can be explained by the expression (23). To this one can notice that in the case of the probing frequency $F = 100$ GHz the three frequencies $\omega, \omega_{ce}, \omega_{pe}$ are very close in the vicinity of the pedestal figure 8. Assuming that $\frac{\omega^2-\omega_{ce}^2}{\omega^2} \ll 1$ and $\frac{\omega^2-\omega_{pe}^2}{\omega^2} \ll 1$ we can infer that $W_{Xturb}^2 \propto \omega^{-4}$. Of course the assumption does not hold in the whole area of the edge turbulence, nevertheless it gives an estimate for the beam width dependence on the frequencies in the certain frequencies range. The real beam width dependence on the frequency is a complicated function of the cyclotron and plasma frequencies profiles, and can be investigated numerically for the given profiles using the expressions (22) and (23). As it was already noted, since the relevant profiles and the turbulence position in the pedestal area are unknown yet, precise investigation is not the object of this study.

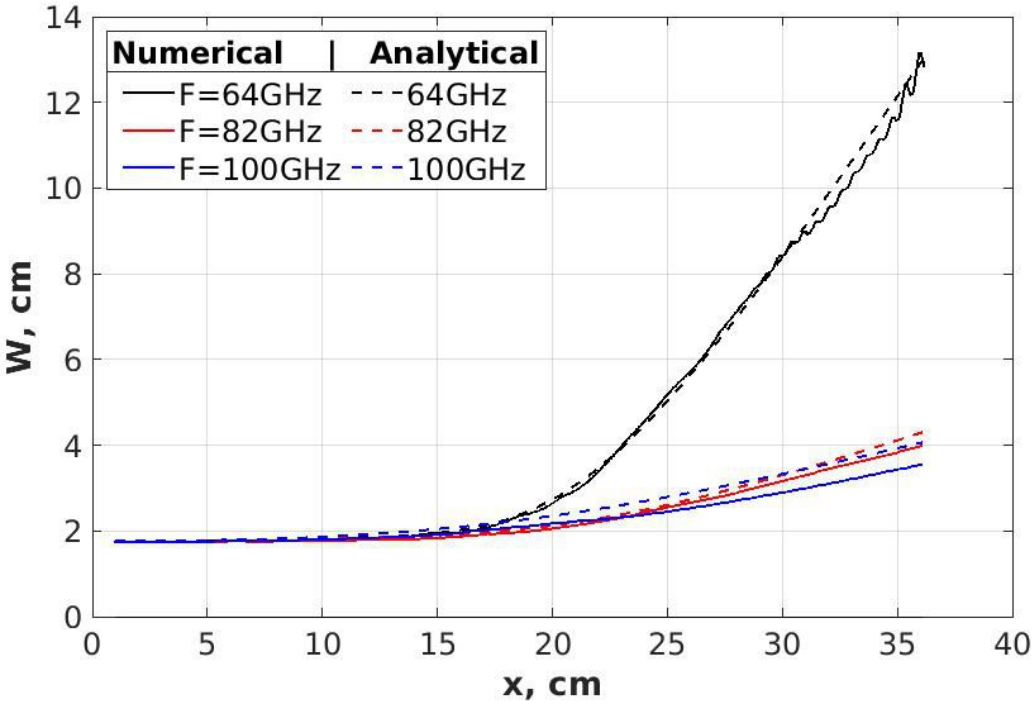


Рис. 7: Comparison of the averaged beam width for different frequencies of a probing beam, turbulence rate $\frac{\delta\tilde{n}_{max}}{n_{max}} = 5.0\%$, correlation length $\lambda_c = 1.6$ cm

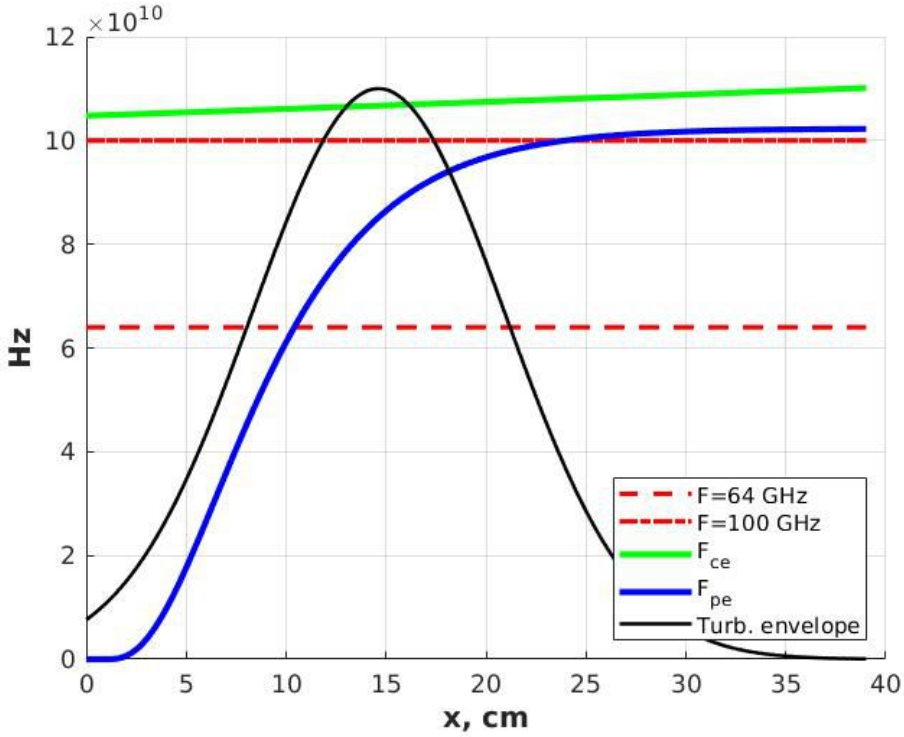


Рис. 8: Profiles of the frequencies F_{ce} and F_{pe}, comparison with the probing frequencies F and position of the turbulence envelope (normalized to 1.1×10^{11})

Simulations under the conditions of ECRH experiment for ASDEX Upgrade

ECRH is a widely used method of plasma heating, normally the heating energy may be deposited at selected location. In the previous studies done [8] a beam ray tracing was used to evaluate the impact of the density fluctuations in particular the enhancement of the power needed to stabilize Neo Classical Tearing modes. In the following works on this subject both polarizations were studied using beam ray tracing and the comparison with a full-wave code was done with O-mode and showed the sensitivity of the beam widening to the turbulence properties [7]. Here to validate the dependencies established in the theoretical part of this paper for X-mode simulations have been performed. These computations were run to investigate the role of the edge turbulence in beam propagation process under conditions of an ECRH experiment. The magnetic field at plasma center $B = 2.5$ T, the maximal value of background density $n_{max} = 0.8 \cdot 10^{20}$ m^{-3}, the probing frequency $F = 140$ GHz provides heating at the second cyclotron harmonic, these characteristics being representative of ASDEX Upgrade. The chosen model profiles are shown on figure 9, an example of the random turbulence distribution is illustrated on figure 10. The correlation length is fixed for these simulation, $\lambda_c = 1.0$

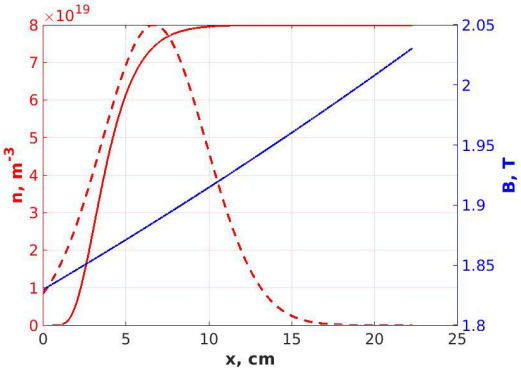


Рис. 9: Solid red and blue curves are density and magnetic field profiles respectively, dashed curve is the envelope of the turbulence $\sqrt{\langle \delta n^2(x) \rangle}$ normalized to the maximal value of the background density

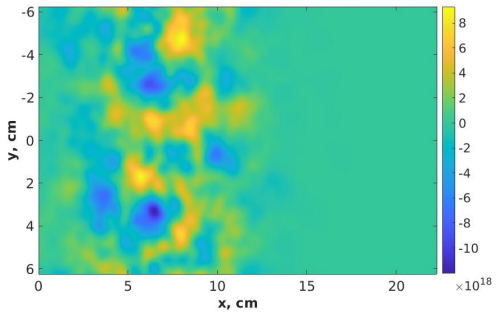


Рис. 10: 2D turbulence map for the follow parameters: turbulence level $\frac{\delta \tilde{n}_{max}}{n_{max}} = 5.0\%$, correlation length λ_c=1.0 cm

cm. The correlation length and turbulence amplitude values are chosen as typical for the tokamak so far as these parameters vary for different regimes [28-30] Moreover the correlation length depends on the radial position [29, 30], but we used a simplified model with a homogeneous turbulence cross-correlation function for the simulations. The beam width evolution for two different turbulence rates: $\frac{\delta \tilde{n}_{max}}{n_{max}} = 5.0\%$ and $\frac{\delta \tilde{n}_{max}}{n_{max}} = 10.0\%$ is obtained numerically and compared with the analytical predictions, see figure 11, the averaging of the numerical distributions is performed over 2600 and 2200 realizations for the two cases respectively. The turbulence level $\frac{\delta \tilde{n}_{max}}{n_{max}} = 5.0\%$ corresponds to the edge of the analytical description applicability, the value $\frac{\delta \tilde{n}_{max}}{n_{max}} = 10.0\%$ is in good agreement with the strong turbulence criteria, checking of the criteria for the two turbulence levels is shown on figure 12.

To know the probabilistic properties of the beam energy allocation in strongly turbulent plasma we investigate the intensity distribution at a fixed position. It is convenient to use the intensity normalized to its average value $I = \frac{E(x,y)^2}{\langle E(x,y)^2 \rangle}$, comparison of the numeri-

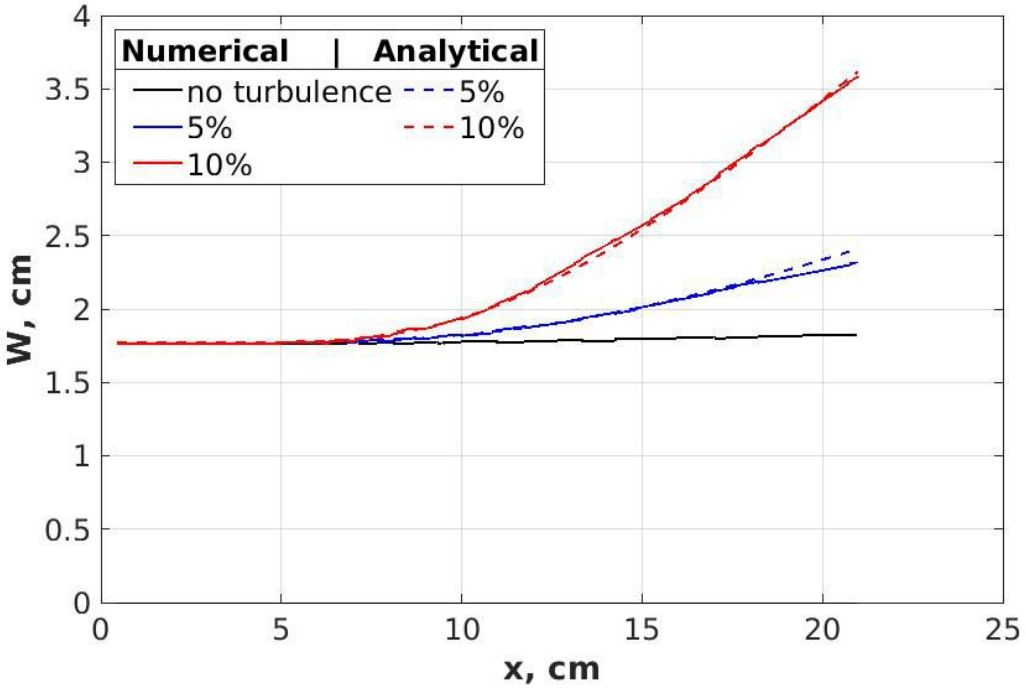


Рис. 11: The averaged beam width evolution in turbulent plasma for fixed turbulence correlation length $\lambda_c = 1.0$ cm and different turbulence rates $\frac{\delta\tilde{n}_{max}}{n_{max}}$ which percentage is specified for each analytical and numerical curve

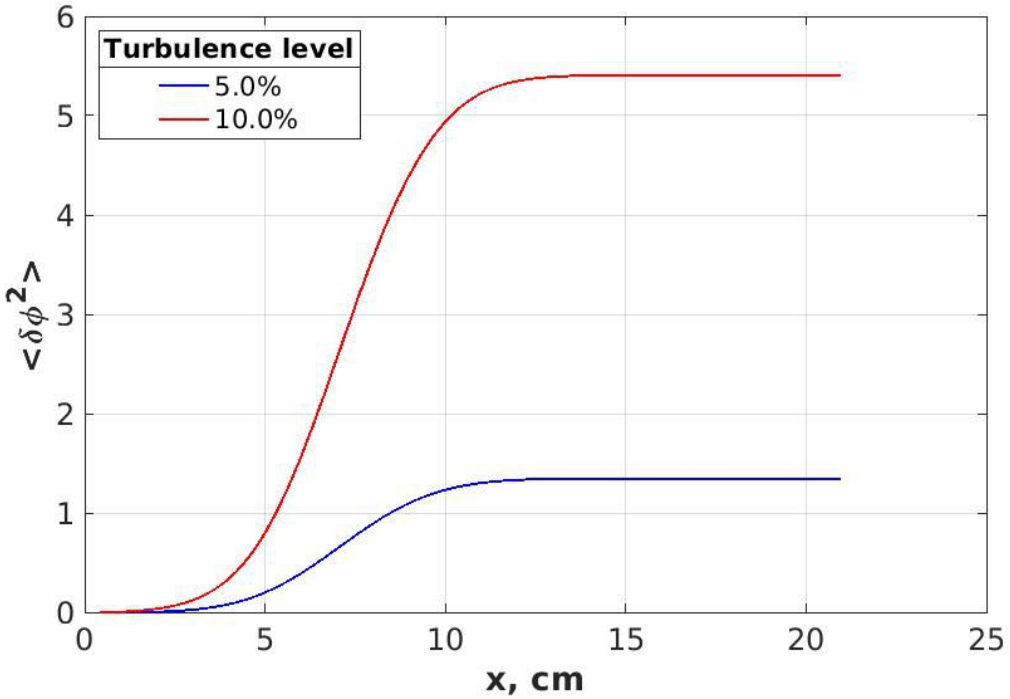


Рис. 12: Averaged square of the phase perturbation for the different turbulence normalized amplitudes $\frac{\delta\tilde{n}_{max}}{n_{max}}$ measured in percentage

cal simulations is provided with the analytical expression (28). For the turbulence level $\frac{\delta\tilde{n}_{max}}{n_{max}} = 5.0\%$ the relative intensity is shown on figures 13 and 14 for the two spacial points: $(x, y) = (20.5, 0)$ cm and $(x, y) = (20.5, 2.3)$ cm respectively. The radial point $x = 20.5$ cm corresponds to the edge of the calculation domain, the two selected poloidal points are positions of the averaged beam axis and width. Analogous simulations are done

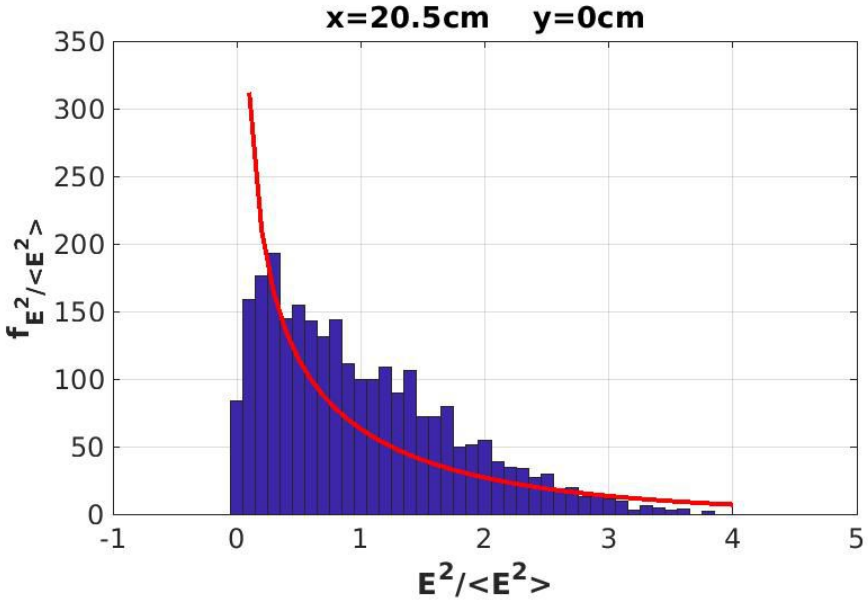


Рис. 13: The intensity distributions, blue histogram is the numerical distribution, red curve is the analytical distribution normalized to the number of realizations. Turbulence level $\frac{\delta\tilde{n}_{max}}{n_{max}} = 5.0\%$, radial position $x = 20.5$ cm at axis of the average beam

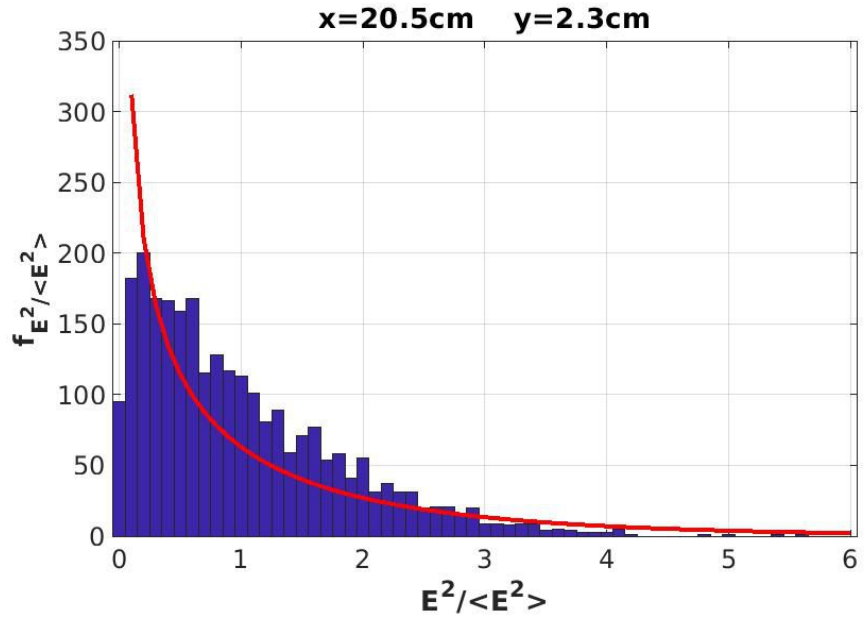


Рис. 14: Intensity distributions, blue histogram is the numerical distribution, red curve is the analytical distribution normalized to the number of realizations. Turbulence level $\frac{\delta\tilde{n}_{max}}{n_{max}} = 5.0\%$, radial position $x = 20.5$ cm at width of the average beam $y = 2.3$ cm

for higher turbulence amplitude $\frac{\delta\tilde{n}_{max}}{n_{max}} = 10.0\%$, the intensity distributions are illustrated on figures 15 and 16 for the points: $(x, y) = (20.5, 0)$ cm and $(x, y) = (20.5, 3.6)$ cm, where the poloidal position $y = 3.6$ cm is width of the averaged beam for this turbulence regime.

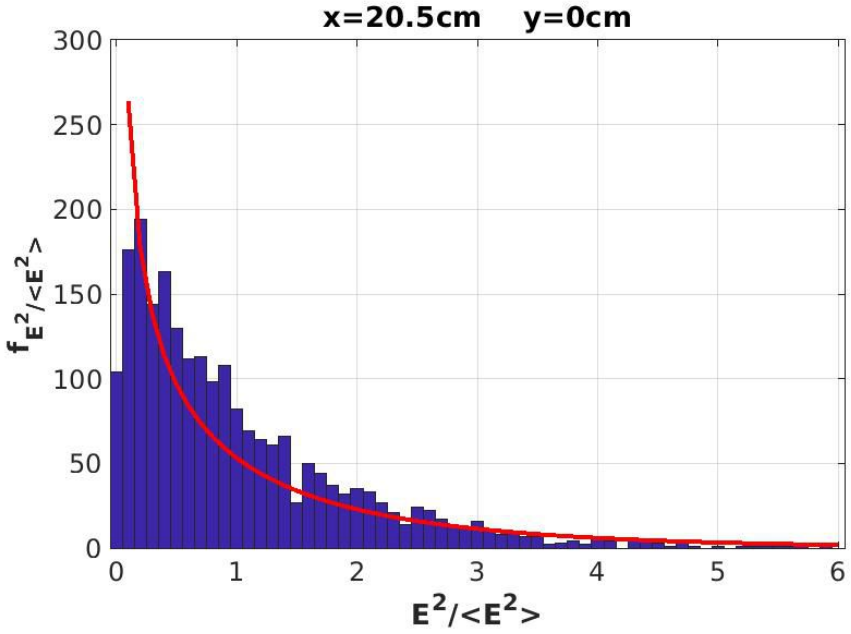


Рис. 15: The intensity distributions, blue histogram is the numerical distribution, red curve is the analytical distribution normalized to the number of realizations. Turbulence level $\frac{\delta\tilde{n}_{max}}{n_{max}} = 10.0\%$, radial position $x = 20.5$ cm at axis of the average beam

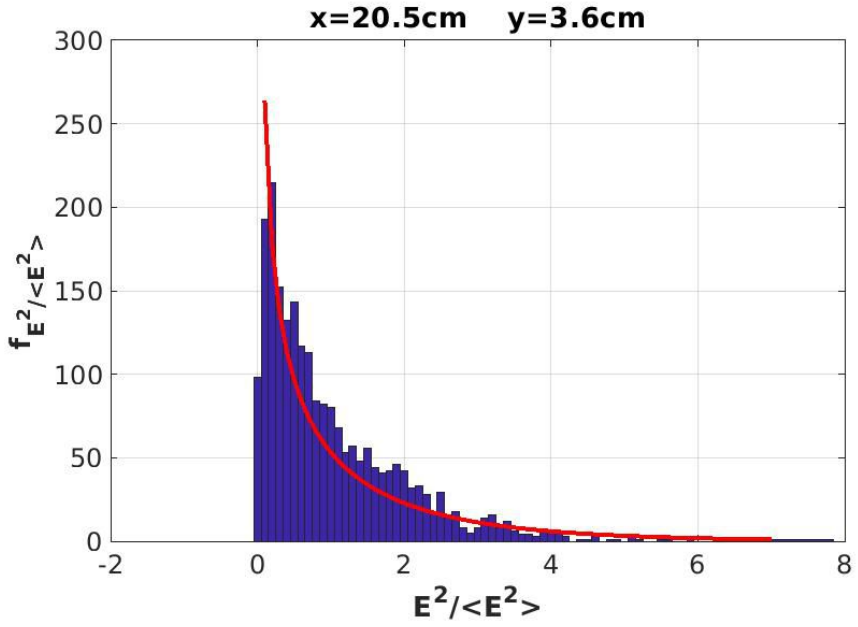


Рис. 16: The intensity distributions, blue histogram is the numerical distribution, red curve is the analytical distribution normalized to the number of realizations. Turbulence level $\frac{\delta\tilde{n}_{max}}{n_{max}} = 10.0\%$, radial position $x = 20.5$ cm at width of the average beam $y = 3.6$ cm

The averaged spatial distribution of a probing microwave beam in turbulent plasma is examined for different scenarios of the turbulence, it is seen that since the strong turbulence regime holds $\langle\delta\phi^2\rangle \gg 1$, results of the numerical simulations are in good agreement with the analytical descriptions for the beam width. According to the figures 13-16, the analytical expression for the intensity probabilistic distribution (28) is able to provide just a relevant estimate of the distribution function profile in the case of the border value of the applicability criterion ($\langle\delta\phi^2\rangle \sim 1$). In this case the average electric field is not negligible (see (26)). The discrepancy between the analytical f_{an} and numerical f_{num} distribution profiles $\frac{f_{an}-f_{num}}{f_{an}}$ depends on a position and constitutes up to 50% in the main area of the distribution function, defined as $\int_0^{\xi^*} f_{num}(\xi)d\xi = 0.99$, other than the vicinity of the point $\xi = \frac{E(x,y)^2}{\langle E(x,y)^2\rangle} = 0$. So far as the simulations number is limited it is impossible to obtain the infinity numerically, which is the analytical prediction. The tail part of the profiles is underestimated in this case. In the case with $\langle\delta\phi^2\rangle \approx 5.4$ the analytical and numerical profiles are in a relatively good agreement. The discrepancy is more homogeneous and its average value $\frac{<f_{an}-f_{num}>}{f_{an}} \approx 18\%$ in the main area. It is seen that the tail part of the distribution is approximated much better than in the low turbulence case.

3 Conclusion.

The microwave X-mode beam propagation in turbulent magnetized plasma is described analytically and simulated numerically, the spatial and probabilistic distributions of the beam are obtained in regime of strong phase modulation of the beam. The main dependencies are given in the Eq. (24), that answers for the X-mode to the question on the sensitivity of the beam widening to the edge turbulence properties. The numerical simulations are performed for plasma conditions characteristic for ITER Baseline Scenario and ASDEX Upgrade, representing model conditions of the CTS and ECRH experiments respectively, with different scenarios of the turbulence. It is shown that under conditions of ITER plasma even low-level edge turbulence may cause significant distortions of beam averaged geometrical characteristics namely beam spatial and angular widths. These results are consistent with the simulations and estimates done previously in [18, 9], the expected additional beam broadening, associated with the edge turbulence, is of the order of 100%. This negative effect may be of high importance for the planned CTS diagnostics in ITER. A CTS diagnostics demands high-power probing beam (of the order of 1MW) due to a very low scattering efficiency, that is why decreasing of the registered signal associated with the plasma edge turbulence can be a noticeable problem. Analysis of the signal measured in a CTS experiment taking into account the edge turbulence will be presented in further work. It should be mentioned that increasing of a probing frequency for the planned CTS experiments in ITER can drastically reduce the negative effect of the beam spreading. The beam distortion associated with the edge turbulence is significant only for a relatively large turbulence amplitude under the condition of ECRH experiment for ASDEX Upgrade. However to evaluate in an accurate manner the effects on the heating systems or diagnostics using microwave beams the knowledge of the turbulence properties (correlation lengths, amplitude) is required, and if it is possible the probing frequency can permit to optimize the spatial resolution taking into account the edge turbulent effects.

Acknowledgements

This work has been carried out within the framework of the the French Federation for Magnetic Fusion Studies (FR-FCM) and EUROfusion Consortium and has received funding from the Euratom research and training program 2014-2018 and 2019-2020 under grant agreement No 633053. The views and opinions expressed herein do not necessarily reflect those of the European Commission. LUE PhD grant of University finances partially this works. Analytical treatment of the beam broadening was also supported by the RSF grant 17-12-01110 whereas the numerical treatment was performed within the state contract of the Ioffe institute.

References

[1] F Leuterer et al, 2003 *Nucl. Fusion* **43** 1329-1342

[2] H Zohm et el., 1999 *Nucl. Fusion* **39(5)** 577-580

[3] S Korsholm et al, 2010 *Nuclear Instruments and Methods in Physics Research A* **623** 677-680

[4] M Hirsch, E Holzhauer, J Baldzuhn, B Kurzan and B Scott, 2001 *Plasma Phys. Control. Fusion* **43** 1641-1660

[5] E V Sysoeva, F da Silva, E Z Gusakov, S Heuraux and A.Yu. Popov, 2015 *Nucl. Fusion* **55(3)** 033016

[6] N Bertelli , G J Kramer and E J Valeo, 2019 *Plasma Phys. Control. Fusion* **61** 105018

[7] A Snicker et al, 2018 *Plasma Phys. Control. Fusion* **60** 014020

[8] E Poli et al, 2015 *Nucl. Fusion* **55** 013023

[9] A Snicker et al, 2018 *Nucl. Fusion* **58** 016002

[10] R J La Haye, 2006 *Phys. Plasmas*, **13** 055501

[11] O. Sauter and et al., 2010 *Plasma Phys. Control. Fusion* **52** 025002

[12] N Bertelli and et al., 2011 *Nucl. Fusion* **51** 103007

[13] M W Brookman, 2017 *EPJ Web of Conferences* **147** 03001

[14] O Chellaï and et al., 2018 *Phys. Rev. Lett.* **120** 105001

[15] I Furno and et al., 2015 *J. Plasma Phys.* **81** 345810301

[16] O. Chellaï and et al., 2017 *EPJ Web of Conferences* **157** 03008

[17] O Chellaï and et al., 2019 *Plasma Phys. Control. Fusion* **61** 014001

[18] C. Tsironis and et al., 2009 *Phys. Plasmas*, **16** 112510

[19] H Weber and et al., 2015 *EPJ Web of Conferences* **87** 01002

[20] A Köhn and et al., 2008 *Plasma Phys. Control. Fusion* **50** 085018

[21] T R N Williams and et al., 2014 *Plasma Phys. Control. Fusion* **56** 075010

[22] COMSOL Multiphysics Reference Manual, 2019 https://doc.comsol.com/5.5/doc/com.comsol.help.comsol/COMSOL_ReferenceManual.pdf

[23] O Chellaï et al, 2021 *Nucl. Fusion* in press https://doi.org/10.1088/1741-4326/abf43f

[24] C Lechte et al, 2017 *Plasma Phys. Control. Fusion* **59** 075006

[25] S B Korsholm et al, 2019 *EPJ Web of Conferences* **203** 03002

[26] T Happel et al, 2017 *Plasma Phys. Control. Fusion* **59** 054009

[27] P Hennequin, R Sabot, C Honoré, et al, 2004 *Plasma Phys. Control. Fusion* **46** B121

[28] A Medvedeva, 2017 "Experimental study of turbulence at the plasma edge of ASDEX Upgrade tokamak with an ultra-fast swept reflectometry"PhD theris TUM

[29] J Schirmer et al, 2007 *Plasma Phys. Control. Fusion* **49** 1019

[30] D Prisiazhniuk et al, 2018 *Plasma Phys. Control. Fusion* **60** 079602